

# 1 RDP3, A Novel Antigout Peptide Derived from Water Extract of Rice

2 Naixin Liu,<sup>||</sup> Ying Wang,<sup>||</sup> Lin Zeng, Saige Yin, Yan Hu, Shanshan Li, Yang Fu, Xinpeng Zhang, Chun Xie,  
 3 Longjun Shu, Yilin Li, Huiling Sun, Meifeng Yang, Jun Sun,<sup>\*</sup> and Xinwang Yang<sup>\*</sup>



Cite This: <https://dx.doi.org/10.1021/acs.jafc.0c02535>



Read Online

ACCESS |



Metrics & More



Article Recommendations



Supporting Information

4 **ABSTRACT:** Gout and hyperuricemia can seriously affect the quality of life; at present, however, existing medicines are unable to  
 5 meet all clinical needs. In the current study, a novel peptide (i.e., rice-derived-peptide-3 (RDP3), AAAAMAGPK-NH<sub>2</sub>, 785.97 Da)  
 6 in water extract obtained from shelled *Oryza sativa* fruits was identified. Testing revealed that RDP3 (minimum effective  
 7 concentration 100 μg/kg) did not show both hemolytic and acute toxicity, and reduced uric acid levels in the serum of  
 8 hyperuricemic mice by inhibiting xanthine oxidase activity and decreasing urate transporter 1 expression. RDP3 also alleviated renal  
 9 injury in hyperuricemic mice by decreasing NLRP3 inflammasome expression. Furthermore, RDP3 alleviated formalin-induced paw  
 10 pain and reduced monosodium urate crystal-induced paw swelling and inflammatory factors in mice. Thus, this newly identified  
 11 peptide reduced uric acid levels and renal damage in hyperuricemic mice and showed anti-inflammatory and analgesic activities,  
 12 indicating the potential of RDP3 as an antigout medicine candidate.

13 **KEYWORDS:** *antigout peptide, nutraceutical peptide, hyperuricemia treatment, renal protective peptides, anti-inflammation peptides*

## 14 ■ INTRODUCTION

15 Gout is a common and complex form of arthritis. It is related  
 16 to purine metabolism disorders, which cause excessive uric acid  
 17 production or poor uric acid excretion, with subsequent  
 18 induction of hyperuricemia (HUA).<sup>1</sup> Clinically, HUA is  
 19 diagnosed when the level of serum uric acid is higher than  
 20 420 μM in men and 360 μM in women.<sup>2</sup> Continuous HUA can  
 21 not only lead to an attack of gouty arthritis but can also cause  
 22 kidney damage, cardiovascular events, and diabetes.<sup>1,3</sup> In  
 23 addition, if HUA is not properly treated and controlled, the  
 24 recurrence, frequency, and degree of gout attack can also  
 25 increase. Therefore, gout is best treated by controlling HUA.<sup>4</sup>  
 26 The concentration of uric acid in the blood is primarily  
 27 determined by the absorption and production of purine and by  
 28 the decomposition and excretion of uric acid.<sup>5</sup> Xanthine  
 29 oxidase (XOD), a key enzyme for the formation of uric acid, is  
 30 a major target of inhibitory drugs<sup>5</sup> such as allopurinol and  
 31 febuxostat.<sup>4</sup> During the process of uric acid metabolism in  
 32 humans, about 65% of uric acid is filtered through the  
 33 glomeruli, with 90% then reabsorbed into circulation through  
 34 urate transporter-related proteins (such as URAT1) and the  
 35 rest filtered into urine for excretion.<sup>5</sup> Antihyperuricemic  
 36 medicines, such as probenecid and benzbromarone, can  
 37 significantly enhance the excretion of uric acid by inhibiting  
 38 URAT1.<sup>6</sup> Currently, the treatment of the acute gout attack  
 39 depends on drugs such as nonsteroidal anti-inflammatory  
 40 drugs (NSAIDs), colchicine, glucocorticoids, and IL-1β  
 41 antagonists.<sup>4</sup> However, their clinical use has several limitations.  
 42 For example, NSAIDs can induce peptic ulcers; allopurinol can  
 43 produce severe skin rash and allergic reactions; febuxostat can  
 44 lead to cardiovascular events; benzbromarone can induce  
 45 hepatotoxic activity; and probenecid can generate uric acid  
 46 crystals in the kidney.<sup>7–10</sup> Therefore, the development of new  
 47 antigout drugs remains an important focus.

In recent years, peptide medicines have attracted increasing 48  
 attention due to their high specificity, high efficiency, limited 49  
 side effects, and low cost.<sup>11–13</sup> At present, the clinical use of 50  
 several peptides, such as exenatide and ACEI, are not only 51  
 more convenient for patients but also provide considerable 52  
 economic benefits for society.<sup>14,15</sup> A large number of other 53  
 active peptides, such as antibacterial, analgesic, and neuro- 54  
 protective peptides, have also been identified.<sup>16,17</sup> To date, 55  
 however, reports on active peptides that can effectively treat 56  
 gout and HUA remain scarce.<sup>11–13,18–20</sup> Therefore, research 57  
 on peptides for gout and HUA treatment is still in its infancy. 58

In this study, a short peptide, named rice-derived-peptide-3 59  
 (RDP3), obtained from the water extract of shelled *Oryza* 60  
*sativa* fruits from Yunnan, China, was identified. The purpose 61  
 of this research was to discover an anti-HUA or antigout 62  
 bioactive peptide from *O. sativa* extract that could be used as a 63  
 potential candidate for the development of antigout drugs. We 64  
 also established a HUA mouse model to explore the 65  
 mechanism and function of the peptide using various 66  
 biochemical experiments (i.e., western blotting and enzyme- 67  
 linked immunosorbent assay (ELISA)). 68

## 69 ■ MATERIALS AND METHODS

**Sample Purification and Synthesis.** *Sample Preparation.* The 70  
 shelled *O. sativa* fruits were obtained from Yunnan province, and 71  
 water extract of shelled *O. sativa* fruits was obtained as follows.<sup>11</sup> The 72

Received: April 21, 2020

Revised: June 15, 2020

Accepted: June 16, 2020

Published: June 16, 2020

73 rice (shelled *O. sativa* fruits, 1 kg) was first soaked in deionized water  
74 (1 L) at 4 °C for 12 h, with the liquid then filtered using a filter paper.  
75 The resulting solution was centrifuged for 20 min at 4 °C and 12  
76 000g, with the supernatant then collected as the water extract of rice.  
77 The obtained liquid was freeze-dried and then stored at -80 °C until  
78 analysis.

79 **Purification Procedures.** Peptide purification was performed as per  
80 our previous report, with some modification.<sup>21</sup> The water extract of  
81 rice was purified using a Sephadex G-50 gel filtration column (1.5 ×  
82 31 cm<sup>2</sup>, superfine, GE Healthcare, Stockholm, Sweden). Then, 25 M  
83 Tris-HCl buffer containing 0.1 M NaCl (pH 7.8) was used for  
84 prebalance and elution at a flow rate of 0.3 mL/min and an injection  
85 volume of 1 mL. The samples were collected (10 min/tube) with an  
86 automatic fractionation collector (BSA-30A, HuXi Company,  
87 Shanghai, China), with absorbance then detected at 280 nm (Figure  
88 S1A, the same as our previous study<sup>10</sup>). The components represented  
89 by the arrow in Figure S1A were collected, combined, and then  
90 injected into a C18 high-performance liquid chromatography  
91 (HPLC) column (Hypersil BDS C18, 4.0 × 300 mm<sup>2</sup>, Elite,  
92 China) at an injection volume of 1 mL, with a detection wavelength  
93 of 220 nm. Ultrapure water with 0.1% (v/v) trifluoroacetic acid  
94 (TFA) was used for prebalancing, and acetonitrile (ACN) with 0.1%  
95 (v/v) TFA was eluted at a flow rate of 1 mL/min through a linear  
96 gradient (0–40% ACN, 40 min, Figure S1B, as shown in our previous  
97 research<sup>10</sup>). The component indicated by an arrow in Figure S1C was  
98 collected and a second round of HPLC was performed as above.

99 **Determination of the Primary Structure of Peptide.** The  
100 molecular mass of the sample was detected by mass spectrometry.  
101 The sample and  $\alpha$ -cyano-4-hydroxycinnamic acid (5 mg/mL,  
102 dissolved in 50% ACN, 0.1% TFA) were mixed to a volume, then 1  
103  $\mu$ L mixture was spotted on a steel plate for crystallization at room  
104 temperature. The crystallized sample on the plate was examined via  
105 mass spectrometry (Autoflex speed TOF/TOF, Bruker Daltonik  
106 GmbH, Leipzig, Germany) for MS and MS/MS analyses in positive  
107 charge mode. The ion source voltages for MS analysis were as follows:  
108 UIS1: 19 kV and UIS2: 16.45 kV. The ion source voltages for MS/MS  
109 analysis were as follows: UIS1: 6 kV and UIS2: 5.15 kV. The reflector  
110 detector voltages for MS and MS/MS data acquisition were set as  
111 1.942 and 2.163 kV, respectively. FlexAnalysis 3.3 and Biotools 3.2  
112 provided by the manufacturer were used for MS and MS/MS spectra  
113 interpretation. Mass tolerance of MS/MS ions was set as  $\pm 0.5$  Da.  
114 The sample was then dissolved in 25 mM NH<sub>4</sub>HCO<sub>3</sub> and reduced  
115 using dithiothreitol at 37 °C for 1 h, and then blocked by  
116 iodoacetamide for 30 min. Finally, the mixture was mixed with  $\alpha$ -  
117 cyano-4-hydroxycinnamic acid and analyzed by tandem mass  
118 spectrometry on the same equipment. The RDP3 peptide  
119 (AAAAMAGPK-NH<sub>2</sub>) was synthesized at a purity of >95% by  
120 Wuhan Bioearegene Biotechnology Co., Ltd. (Wuhan, China).

121 **Animal Care.** Kunming and nude mice (25  $\pm$  5 g) were obtained  
122 from Hunan Slack Jingda Laboratory Animal Co., Ltd. (Hunan,  
123 China). All mice were housed in cages (330 × 205 × 180 mm<sup>3</sup>, five  
124 mice per cage) at room temperature (22  $\pm$  2 °C), with free access to  
125 food and water. All animal handling was implemented in accordance  
126 with the Provisions and General Recommendations of the Chinese  
127 Experimental Animals Administration Legislation. All animal care and  
128 handling procedures were conducted in accordance with the  
129 requirements of the Ethics Committee of Kunming Medical  
130 University (KMMU20180012).

131 **Characteristics of RDP3. Hemolytic Activity and Acute Toxicity**  
132 **Assays.** Hemolytic activity was examined as per earlier experiments,  
133 with some modifications.<sup>22</sup> First, human red blood cells (Kunming  
134 Blood Center, Kunming, Yunnan, China) were mixed with saline and  
135 centrifuged at 3000g for 5 min at 4 °C to obtain 100% red blood cells.  
136 The saline was used as the solvent. Different doses of RDP3 (500  $\mu$ L,  
137 100  $\mu$ g/mL, 500  $\mu$ g/mL, 1 mg/mL) were gently mixed with the red  
138 blood cells (500  $\mu$ L) and incubated at 37 °C for 30 min. The mixture  
139 was then centrifuged at room temperature (22  $\pm$  2 °C) for 4 min at  
140 4000g. Finally, the supernatant was tested at 540 nm, with 0.1%  
141 Triton X-100 used as the positive control to determine the maximum  
142 hemolysis rate ( $n = 5$ ).

Acute toxicity was investigated following previous research.<sup>22</sup> 143  
Briefly, different doses of RDP3 (100  $\mu$ g/kg, 500  $\mu$ g/kg, 1 mg/kg) 144  
and saline (1 mL/kg) were injected into the abdominal cavity of mice. 145  
The mortality and general situation of animals in each group were 146  
observed and recorded within 24 h ( $n = 3$ ). 147

**Stability of RDP3.** The stability of RDP3 was determined according 148  
to previous research, with some modifications.<sup>21</sup> In brief, 100  $\mu$ L of 149  
mouse plasma and 100  $\mu$ L of RDP3 (10  $\mu$ g/mL) were mixed, 150  
incubated at 37 °C, and then tested every 2 h. To terminate the 151  
reaction, 219  $\mu$ L of urea (8 M) and 60  $\mu$ L of trichloroacetic acid (1 g/  
152 mL) were added to the mixture. The supernatant was obtained by  
153 centrifuging the mixture at 12 000g for 30 min at 4 °C, which was  
154 then collected to determine the peptide amount using HPLC. 155

After the prepared solution (containing RDP3, 10  $\mu$ g/mL) was 156  
repeatedly frozen overnight (at -20 °C) and thawed (at 37 °C), the 157  
residual content of the peptide was detected by HPLC. Its stability 158  
under different temperatures was also researched. Specifically, RDP3 159  
(10  $\mu$ g/mL) was incubated at 4, 37, and 60 °C for 20 days, with  
160 samples collected every 2 days. After centrifugation at 12 000g for 20  
161 min at 4 °C, the supernatant was collected and tested using HPLC. 162

RDP3 stability tests were determined by HPLC. In summary, the 163  
samples (an injection volume of 1 mL) were tested using a C18 164  
HPLC column prebalanced with ultrapure water containing 0.1% (v/  
165 v) TFA and with ACN containing 0.1% (v/v) TFA. Elution was  
166 conducted at a flow rate of 1 mL/min (0–30% ACN, 30 min) and  
167 monitored at 220 nm. Peak area (elution time) chromatography was  
168 used to determine and quantify RDP3 residue. 169

**Distribution of RDP3 In Vivo after Injection.** The fluorescein- 170  
isothiocyanate-AAAAMAGPK-NH<sub>2</sub> (FITC-RDP3) sample was pro- 171  
vided commercially by Wuhan Bioearegene Biotechnology Co., Ltd. 172  
(Wuhan, China). First, nude mice were anesthetized with 173  
pentobarbital sodium (3.5%, 100  $\mu$ L/10 g) and fixed, followed by 174  
abdominal injection of 100  $\mu$ L of FITC-RDP3 (10  $\mu$ g/ $\mu$ L). Front and 175  
back images of mice were then taken and examined at 0 and 60 min 176  
after the injection using a FluorVivo300 (Huanya Technology Co., 177  
Ltd., Beijing, China). 178

**Antihyperuricemic Activity of RDP3. Establishment of HUA** 179  
**Mice.** Animal assays were performed according to previous research.<sup>23</sup> 180  
Mice were randomly divided into various groups, namely, control, 181  
model, allopurinol (Allo, positive group), benzbromarone (Benz, 182  
positive group), and RDP3 groups (100  $\mu$ g/kg, 500  $\mu$ g/kg, and 1 mg/  
183 kg). From day 1 to 7, the mice in the control group were given 1 mL  
184 of saline per day, whereas the other groups were treated with  
185 intragastric administration of 300 mg/kg potassium oxonate (POX,  
186 Dalian Meilun Biological Technology Co., Ltd., Dalian, Liaoning,  
187 China) and 200 mg/kg adenine (Dalian Meilun Biological  
188 Technology Co., Ltd., Dalian, Liaoning, China) per day. One hour  
189 after POX and adenine treatment, saline was given to mice in the  
190 control and model groups, whereas the positive groups were treated  
191 with the intraperitoneal injection of Allo (10 mg/kg, Dalian Meilun  
192 Biological Technology Co., Ltd., Dalian, Liaoning, China) or Benz (8  
193 mg/kg, Dalian Meilun Biological Technology Co., Ltd., Dalian,  
194 Liaoning, China) and the RDP3 groups were treated with the  
195 intraperitoneal injection of different doses of RDP3 (100  $\mu$ g/kg, 500  
196  $\mu$ g/kg, and 1 mg/kg). Blood and tissue samples were obtained on day  
197 7 after the last administration of RDP3, Allo, or saline. Briefly, 1 h  
198 after the last administration, the mice were anesthetized with 0.3%  
199 pentobarbital sodium and blood was taken from the inner canthus  
200 vein, followed by the rapid removal of liver and kidney tissues on ice.  
201 The whole blood samples were centrifuged at 6000g for 5 min at  
202 room temperature (22  $\pm$  2 °C) to obtain serum. The kidneys and  
203 livers of mice were stored at -80 °C, with portions of the kidneys  
204 fixed in 4% formaldehyde. 205

**Detection of Uric Acid and Creatinine Levels in HUA Mice.** Serum 206  
levels of uric acid and creatinine were measured using uric acid and 207  
creatinine kits as per the manufacturer's operational instructions 208  
(Nanjing Jiancheng Bioengineering Institute, Nanjing, Jiangsu,  
209 China). 210

**Hematoxylin and Eosin (H&E) Staining.** H&E staining was 211  
performed according to the prior study.<sup>11</sup> Kidneys of mice were fixed 212

213 in 4% formalin for 24–48 h, then dehydrated using gradient ethanol  
214 (75% 12 h, 85% 12 h, 95%, and 100% 2 h, respectively). Tissues were  
215 then embedded in paraffin and sliced to a thickness of 5  $\mu\text{m}$ , followed  
216 by H&E staining and visualization via light microscopy (Zeiss,  
217 Germany) at 100 $\times$  magnification.

218 **Molecular Docking.** Molecular docking of RDP3-XOD and RDP3-  
219 URAT1 complexes was conducted to explore the mechanism related  
220 to the lowering of uric acid by RDP3.<sup>24</sup> Briefly, the X-ray crystal  
221 structure of XOD was downloaded from the Protein Data Bank  
222 (PDB-ID: 2ckj) (<http://www.rcsb.org/pdb>). The URAT1 architec-  
223 ture was modeled from scratch using the Robetta server (<http://www.robetta.org/>). The RDP3 structure was constructed using the PEP-  
224 FOLD3 server ([http://bioserv.rpbs.univ-paris-diderot.fr/services/](http://bioserv.rpbs.univ-paris-diderot.fr/services/PEP-FOLD3/)  
225 [PEP-FOLD3/](http://bioserv.rpbs.univ-paris-diderot.fr/services/PEP-FOLD3/)). Vina 1.1.2 was used for molecular docking, and the  
226 conformation with the best affinity (lowest value) was chosen as the  
227 docking conformation. The results were then analyzed using Pymol  
228 and DS3.5 software.

230 **Detection of XOD In Vivo and In Vitro.** XOD activity in the serum  
231 and liver of HUA mice was measured using specific XOD kits  
232 (Nanjing Jiancheng Bioengineering Institute, Nanjing, Jiangsu,  
233 China), and the IL-1 $\beta$  level in the serum of mice was tested using  
234 mouse IL-1 $\beta$  ELISA kits (Shenzhen NeoBioscience Biotechnology  
235 Co., Ltd., Shenzhen, China) following the instructions provided by  
236 the manufacturer.

237 XOD inhibition *in vitro* was carried out following previous research,  
238 with some modifications.<sup>12</sup> Tris–HCl (pH = 8) buffer (50 mM) was  
239 prepared as the solvent. Then, 2 mM of xanthine (Dalian Meilun  
240 Biological Technology Co., Ltd., Dalian, Liaoning, China) and 0.52  
241 mM of XOD (Dalian Meilun Biological Technology Co., Ltd., Dalian,  
242 Liaoning, China) solutions were, respectively, dissolved in the above  
243 solvent. The xanthine solution (128  $\mu\text{L}$ ), XOD solution (16  $\mu\text{L}$ ),  
244 RDP3 solution (32  $\mu\text{L}$ , 100  $\mu\text{g}/\text{kg}$ , 500  $\mu\text{g}/\text{kg}$ , and 1 mg/kg), and  
245 Tris–HCl buffer (928  $\mu\text{L}$ ) were mixed and incubated at 37  $^{\circ}\text{C}$  for 15  
246 min. Afterward, 48  $\mu\text{L}$  of 1 M HCl was used to terminate the reaction,  
247 with absorbance then detected at 292 nm. Allo (10 mg/mL) and  
248 Tris–HCl buffer were used as the positive and negative controls,  
249 respectively. Inhibitory activity was calculated as follows

$$\text{XOD inhibition rate (\%)} = 100\% \times \frac{\text{negative control} - \text{sample}}{\text{negative control}}$$

250 **Detection of IL-1 $\beta$  Levels in the Serum of HUA Mice.** The IL-1 $\beta$   
251 levels in the serum of mice were tested using mouse IL-1 $\beta$  ELISA kits  
252 (Shenzhen NeoBioscience Biotechnology Co., Ltd., Shenzhen, China)  
253 following the instructions provided by the manufacturer.

254 **Western Blotting.** Western blot analysis was performed following  
255 the previous study.<sup>25</sup> Protein from kidney samples was extracted using  
256 20 mg/150  $\mu\text{L}$  radio immunoprecipitation assay (RIPA) and  
257 phenylmethylsulfonyl fluoride (PMSF) (Dalian Meilun Biotechnology  
258 Co., Ltd., Dalian, Liaoning, China) at a ratio of 100:1 following the  
259 manufacturer-provided instructions. A BCA protein analysis kit  
260 (Dalian Meilun Biotechnology Co., Ltd., Dalian, Liaoning, China)  
261 was used to detect the protein content. Sulfate polyacrylamide gel  
262 electrophoresis (SDS-PAGE) was performed to detect the URAT1  
263 and NLRP3 inflammasome contents in the kidneys. The protein was  
264 separated by 10% SDS-PAGE and transferred to poly(vinylidene  
265 fluoride) (PVDF) membranes. After sealing with 5% skimmed milk  
266 for 2 h, the membranes were incubated with primary antibody  
267 (GAPDH, URAT1, NLRP3, ASC, Caspase-1, Proteintech, Shanghai  
268 Sixin Biotechnology Co., Ltd., Shanghai, China) overnight at 4  $^{\circ}\text{C}$ ,  
269 and then with secondary antibody (anti-rabbit, Proteintech, Shanghai  
270 Sixin Biotechnology Co., Ltd., Shanghai, China) for 1 h at room  
271 temperature (22  $\pm$  2  $^{\circ}\text{C}$ ). Membranes were finally analyzed and  
272 quantified using Image J software.

273 **Antigout Activity of RDP3. Anti-Inflammatory and Analgesic**  
274 **Activities of RDP3.** As per the previous research,<sup>26</sup> mice were  
275 pretreated with saline, diclofenac sodium (DS, 12 mg/kg), or different  
276 concentrations of RDP3 (100  $\mu\text{g}/\text{kg}$ , 500  $\mu\text{g}/\text{kg}$ , and 1 mg/kg) via  
277 intraperitoneal injection. Saline was used as a negative control and DS  
278 was used as a positive control. After 30 min, mice were injected with

279 20  $\mu\text{L}$  of 0.92% formalin under the skin of the right paw and then  
280 placed in cages (20  $\times$  40  $\times$  15  $\text{cm}^3$ ) individually. Time spent licking  
281 the paw by each mouse was recorded (0–5 and 15–30 min after  
282 injection).

283 Monosodium urate (MSU) crystals were prepared according to the  
284 previous research.<sup>27</sup> Mice were divided into five groups ( $n = 6$ ): i.e.,  
285 (1) the model group, treated with saline; (2) the positive group,  
286 treated with 12 mg/kg DS; (3) the RDP3 group, treated with different  
287 concentrations of RDP3 (100  $\mu\text{g}/\text{kg}$ , 500  $\mu\text{g}/\text{kg}$ , and 1 mg/kg,  
288 respectively). The mice received an intraperitoneal injection once  
289 daily. On day 3, 30 min after injection, MSU crystals (20 mg/mL)  
290 were injected into the left paw of mice. Subsequent inflammation was  
291 quantified by measuring paw thickness with a digital thickness gauge  
292 (Hong Kong Dinghao Measuring Tool Co., Ltd., Hong Kong, China)  
293 on days 1, 2, and 3 after MSU crystal injection. The percentage of  
294 edema was calculated as follows:

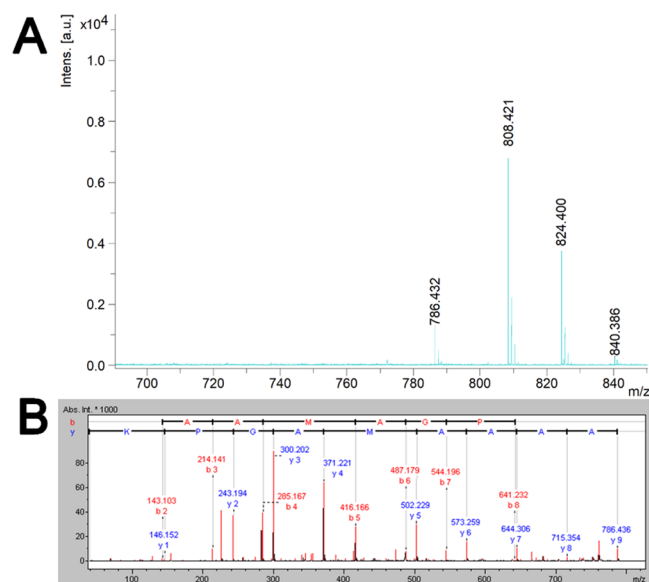
$$\text{result} = 100\% \times \left( \frac{b - a}{a} \right)$$

where “a” is the paw thickness before MSU crystal injection and “b” is  
295 the paw thickness after MSU crystal injection.

296 **Paw Inflammation Cytokine Assays and H&E Staining.** The  
297 levels of IL-1 $\beta$  and TNF- $\alpha$  in mouse feet were tested using specific  
298 mouse IL-1 $\beta$  and TNF- $\alpha$  ELISA kits (Shenzhen NeoBioscience  
299 Biotechnology Co., Ltd., Shenzhen, China). All operations were  
300 carried out according to the instructions provided by the  
301 manufacturer. H&E staining was performed following the procedures  
302 used for kidneys, with treated sections visualized via light microscopy  
303 (Zeiss, Germany) at 100 $\times$  magnification.

## 305 RESULTS AND DISCUSSION

306 **Separation and Identification of RDP3 from Shelled**  
307 **O. sativa Fruits.** Water extract from shelled *O. sativa* fruits  
308 was separated using a Sephadex G-50 gel filtration column.  
309 The sample indicated by an arrow in Figure S1A (Figure 1A in  
310 previous research<sup>11</sup>) was collected and further separated and  
311 purified by RP-HPLC, as shown in Figure S1B. The sample  
312 indicated by an arrow in Figure S1B (corresponding to Figure  
313 1B in previous research,<sup>11</sup> but with different separation peaks)  
314 was again purified using HPLC to obtain the sample with an



315 **Figure 1.** Structure of RDP3. (A) Molecular weight of RDP3 (785.97  
316 Da). (B) Primary structure of RDP3 (AAAAMAGPK-NH<sub>2</sub>).

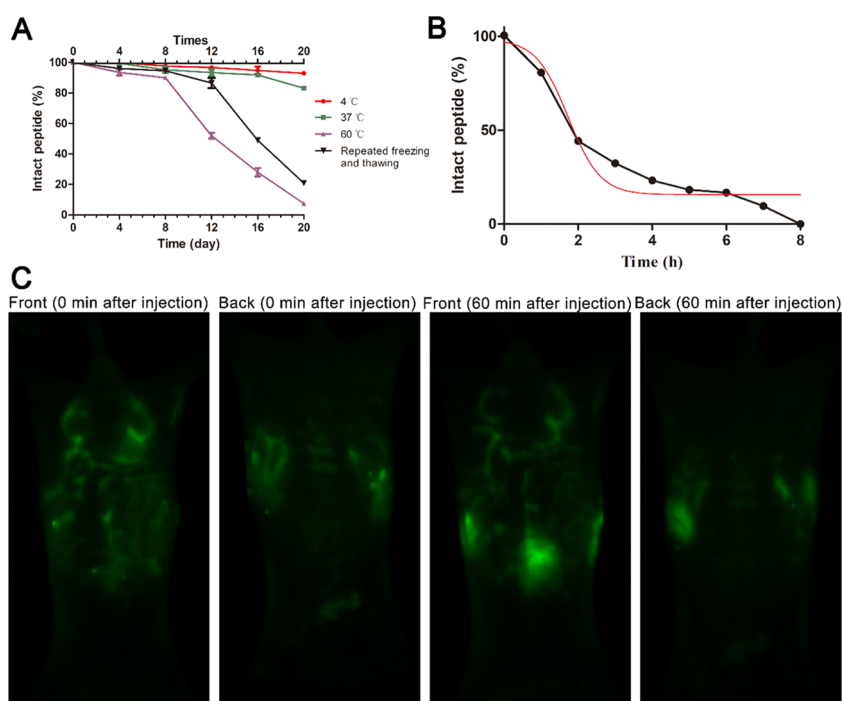


**Figure 2.** Characteristics of RDP3. (A) RDP3 showed great stability at 4, 37, and 60 °C and during repeated freezing and thawing ( $n = 3$ ). (B) Half-life of RDP3 incubated with plasma was 1.7 h, with complete degradation within 8 h ( $n = 3$ ). (C) Images after injection of FITC-RDP3.

315 elution time of 16.8 min (as shown in Figure S1C). The final  
316 sample was analyzed by mass spectrometry.

317 As shown in Figure 1A, a peptide triplet with a single isotope  
318  $m/z$  of 786.432–808.421–824.400 was observed in the  
319 sample. Tandem mass spectrometry was further used to  
320 elucidate the sequence of the peptide triplet. The MS/MS  
321 spectra showed that the mother ions with  $m/z$  of 786.432,  
322 808.421, and 824.400 represented the  $[M + H]^+$ ,  $[M + Na]^+$ ,  
323 and  $[M + K]^+$  types, respectively (Figure 1B), confirming that  
324 the sequence of the sample was “AAAAMAGPK-NH<sub>2</sub>”.

325 **RDP3 Showed No Hemolytic Activity or Acute**  
326 **Toxicity.** To evaluate the safety of RDP3, hemolytic activity  
327 and acute toxicity were tested. As shown in Tables S1 and S2,  
328 RDP3 showed no such activity or toxicity.

329 **Stability of RDP3 and Distribution in Liver and**  
330 **Kidney after Injection.** To explore the characteristics of  
331 RDP3, its stability under different conditions was measured. As  
332 shown in Figure 2A, after repeated freezing and thawing (12  
333 times), the nondegraded content of RDP3 in the prepared test  
334 solution was about 80%; after 20 times, however, the RDP3  
335 content was completely degraded. After 20 days, the content of  
336 RDP3 at 4 and 37 °C was stable, with the residual content of  
337 90 and 80%, respectively. After 20 days at 60 °C, the residual  
338 RDP3 content was about 20%. The stability of RDP3 in plasma  
339 was also tested. As shown in Figure 2B, after incubation with  
340 plasma for 8 h, RDP3 was completely degraded, with a half-life  
341 of 1.7 h (calculated using GraphPad Prism software).

342 FITC-RDP3 was synthesized to observe peptide distribution  
343 in mice after injection. As shown in Figure 2C, after  
344 intraperitoneal injection, the peptide was rapidly distributed  
345 to the whole intraperitoneal area. Front and back images of the  
346 mice were obtained by *in vivo* fluorescence imaging. The  
347 results showed that 60 min after injection, the peptide was  
348 mainly distributed in the abdominal cavity of mice, especially  
349 the liver and kidney.

The novel antihyperuricemic peptide RDP1 (AAAAGA- 350  
KAR), identified in the previous study, shows complete 351  
degradation in plasma at 20 min, with a half-life of 4.6 352  
min.<sup>11</sup> In this research, RDP3 showed increased plasma 353  
stability (half-life: 1.7 h), which may be due to its post- 354  
translation modification (–NH<sub>2</sub>). Stability testing under other 355  
conditions also confirmed better stability of RDP3 compared 356  
with RDP1. Thus, RDP3 showed characteristics of long-term 357  
maintenance at 4 and 37 °C and short-term maintenance at 60 358  
°C, which is a good advantage for its transportation and 359  
preservation. Moreover, its excellent stability in plasma also 360  
suggests good long-term maintenance *in vivo*. 361

**RDP3 Significantly Decreased Serum Uric Acid and**  
362 **Alleviated Renal Damage.** As the biochemical basis of gout, 363  
uncontrolled HUA can lead to the accumulation of uric acid 364  
crystals in the kidney as well as serious renal damage.<sup>28,29</sup> To 365  
understand the anti-HUA and nephrotic activity of RDP3, a 366  
HUA mouse model was established by POX and adenine 367  
treatment to simulate the pathological characteristics of HUA 368  
(*e.g.*, increase in serum uric acid level and renal damage).<sup>5</sup> As 369  
shown in Figure 3A, serum uric acid levels were significantly 370  
higher in the model group ( $65.0 \pm 5.2$  mg/L) than in the 371  
control group ( $23.4 \pm 1.8$  mg/L) ( $P < 0.001$ ), indicating the 372  
successful establishment of HUA in mice. Serum uric acid 373  
levels were significantly lower in the Allo and Benz groups than 374  
in the HUA mice ( $P < 0.001$ ). Serum uric acid concentrations 375  
in the RDP3 groups (100  $\mu$ g/kg, 500  $\mu$ g/kg, and 1 mg/kg) 376  
were  $54.0 \pm 0.7$ ,  $44.2 \pm 0.3$ , and  $39.5 \pm 0.4$  mg/L, respectively 377  
( $P < 0.001$  vs model). These results show that RDP3 had the 378  
ability to reduce serum uric acid levels, with the effects found 379  
to be concentration dependent. Moreover, RDP3 (1 mg/kg) 380  
showed similar effects as the positive control, but at a much 381  
lower dosage. 382

As shown in Figure 3B, the serum creatinine level in the 383  
model group was about seven times higher than that in the 384  
control group ( $P < 0.001$  vs control on day 7), whereas the 385

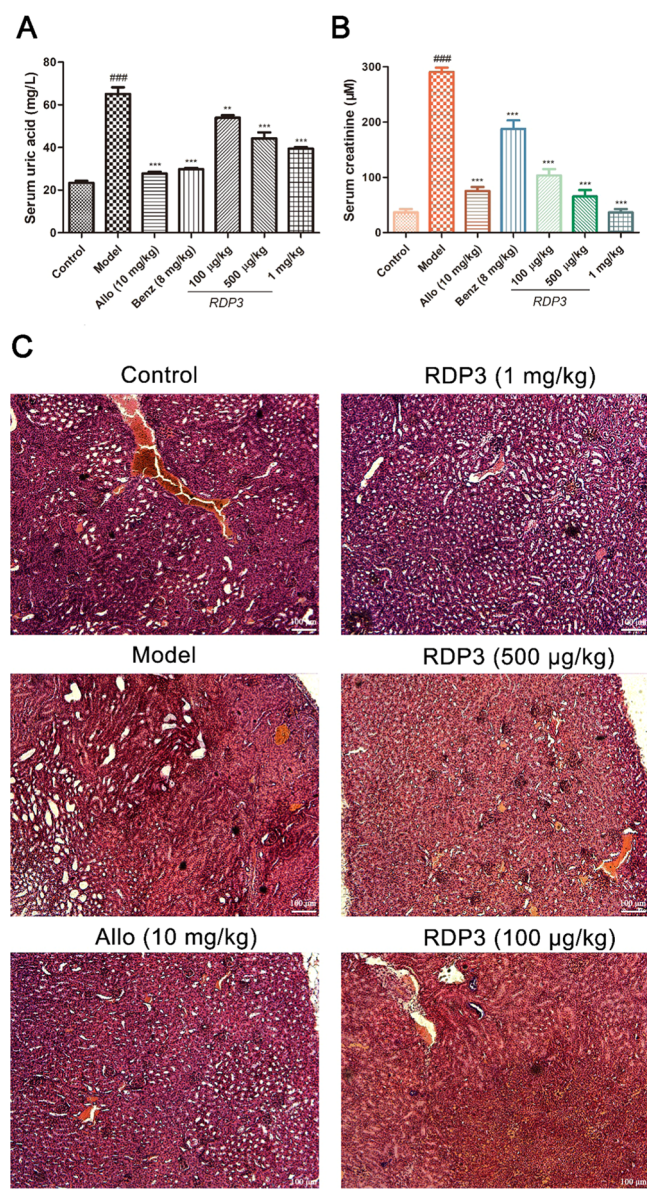


**Figure 3.** RDP3 reduced uric acid level and alleviated kidney damage in hyperuricemic mice. (A) RDP3 induced a concentration-dependent decrease in serum uric acid in hyperuricemic mice ( $n = 6$ ). (B) RDP3 significantly reduced serum creatinine levels in mice ( $n = 6$ ). (C) Control group showed orderly arranged epithelial cells. The model group showed the disappearance of brush border and tubular atrophy, with RDP3 and Allo treatment relieving renal injury. ###/\*\*\* $P < 0.001$  are significantly different from the control (Student's  $t$ -tests).

serum creatinine levels in the Allo (12 mg/kg) and Benz groups (8 mg/kg) were significantly lower ( $P < 0.001$  vs model on day 7). The serum creatinine levels in the RDP3 groups (100 μg/kg, 500 μg/kg, and 1 mg/kg) were  $103.5 \pm 36.9$ ,  $65.3 \pm 24.2$ , and  $36.5 \pm 3.2$  μM, respectively. Thus, RDP3 reduced serum creatinine levels in a concentration-dependent manner. In addition, RDP3 at 1 mg/kg showed stronger activity than that of Allo and Benz. Furthermore, RDP3 at 500 and 100 μg/kg showed stronger renal function improvement ability than Benz at 8 mg/kg.

H&E staining was performed to evaluate the ability of RDP3 to alleviate renal injury at the tissue level. As shown in Figure 3C, the renal tubule borders in the control group were clear and epithelial cells showed ordered arrangement. In contrast,

the kidneys of HUA mice showed indistinct boundaries between the adjacent proximal convoluted tubules, as well as tubular atrophy. These findings are consistent with the serum creatinine results, with RDP3 and positive control treatment relieving the renal pathological changes observed in HUA mice.

In HUA animals, RDP1 and RDP3 reduced uric acid levels by  $49.7 \pm 2.2$  and  $39.2 \pm 0.6\%$ , respectively, suggesting that RDP3 had a weaker ability at reducing uric acid than RDP1 (1 mg/kg) (100% for the model group). In contrast, RDP3 decreased creatinine levels by almost twice that of RDP1, i.e.,  $86.0 \pm 1.1$  and  $41.3 \pm 8.8\%$ , respectively (100% for the model group). Both Allo and Benz are considered first-line drugs for the rapid clinical treatment of excess uric acid.<sup>8</sup> Here, at a low concentration of 1 mg/kg, RDP3 showed a similar reduction in uric acid as produced by the positive control, but with far better renal protective ability than either Allo or Benz (12 and 8 mg/kg). In addition, given its safe extraction from edible rice, the risk of adverse reactions to RDP3 is low. Thus, RDP3 exhibits great potential as a drug candidate against HUA, especially in the treatment of HUA-related nephropathy.

**RDP3 Inhibited XOD Activity and URAT1 Expression in Mice.** Uric acid is the final product of purine metabolism. Under normal physiological conditions, purine is metabolized in the liver via enzymatic action, e.g., XOD, with the resulting uric acid predominantly excreted via the kidney in urine. Renal transporters in proximal convoluted tubules, e.g., URAT1, play important roles in this process. To elucidate the mechanism related to the reduction of uric acid by RDP3, molecular docking of RDP3 with XOD and URAT1 was performed. As shown in Figure S2A–D, RDP3 was combined in the larger cavity of XOD with a curl conformation. The combination of RDP3 and URAT1, as is shown in Figure S2E–H, results demonstrated that RDP3 combined with the hydrophobic core surrounded by the spiral structure of URAT1, which formed three hydrogen bonds. The affinities of RDP3 with XOD and URAT1 were  $-8.0$  and  $-8.6$  kcal/mol, respectively (lower affinity indicates better binding).

Both the XOD activity and URAT1 content were detected in HUA mice. As shown in Figure 4A, the XOD activity levels in the control, model, and Allo groups were  $28.5 \pm 0.5$ ,  $32.1 \pm 0.4$ , and  $19.8 \pm 0.5$  U/L, respectively ( $P < 0.001$ , control vs model;  $P < 0.001$  Allo vs model). The XOD activity levels in the RDP3 groups (100 μg/kg, 500 μg/kg, and 1 mg/kg) were  $28.6 \pm 0.4$ ,  $27.8 \pm 1.0$ , and  $23.4 \pm 1.4$  U/L, respectively. These results suggest that RDP3 treatment effectively reduced XOD activity in HUA mice in a concentration-dependent manner, as confirmed by XOD activity in the liver of HUA mice (Figure 4B).

The direct interaction of RDP3 with XOD *in vitro* was also detected. As shown in Figure S3, RDP3 inhibited XOD concentration dependently. Notably, the XOD inhibitory ability of RDP3 (1 mg/kg) *in vivo* was similar to that of Allo (10 mg/kg), whereas the XOD inhibitory rate *in vitro* (RDP3, 1 mg/mL,  $29.45 \pm 11.15\%$ ) was only a quarter of that of Allo (10 mg/mL,  $99.97 \pm 0.44\%$ ). As reported in previous research, short peptides can be easily degraded into smaller peptide sequences *in vivo*.<sup>12</sup> Therefore, it is possible that RDP3 was degraded into shorter peptide sequences *in vivo*, and its ability to inhibit XOD was enhanced accordingly.

Based on western blotting, the expression of URAT1 in the kidney of HUA mice was also detected. As shown in Figure 4C, compared with the control group, the expression of

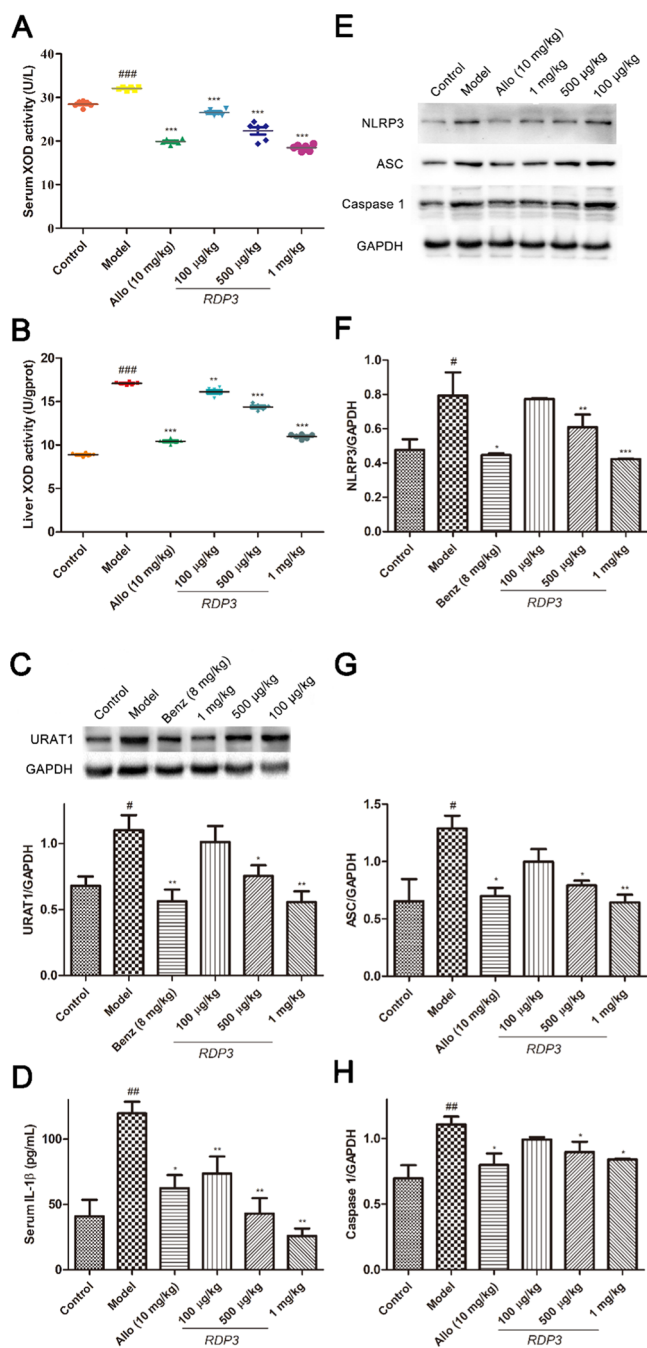


**Figure 4.** RDP3 decreased XOD activity and showed anti-inflammatory activity in mice. RDP3 decreased XOD activity in serum (A) and liver (B) in a concentration-dependent manner ( $n = 6$ ), and decreased expression of URAT1 in kidneys (C,  $n = 3$ ). (D) RDP3 (100  $\mu$ g/kg, 500  $\mu$ g/kg, and 1 mg/kg) decreased the serum levels of IL-1 $\beta$  in mice in a concentration-dependent manner. NLRP3 inflammasome expression levels in hyperuricemic mice were detected by western blot analysis, followed by quantitative analysis (E) ( $n = 3$ ). F–H show quantitative analysis results, in which RDP3 reduced NLRP3 inflammasome expression (NLRP3, ASC, and caspase-1). #/\* $P < 0.05$ , ##/\*\* $P < 0.01$ , and ###/\*\* $P < 0.001$  are significantly different from the control (Student's  $t$ -tests).

463 URAT1 in the model group increased significantly, whereas  
464 under RDP3 intervention (500  $\mu$ g/kg and 1 mg/kg), the  
465 expression of URAT1 in the kidney of HUA mice decreased  
466 significantly, suggesting that RDP3 reduced uric acid by

inhibiting the expression of URAT1. These results also suggest  
467 that RDP3 may target XOD and URAT1 at the same time to  
468 reduce uric acid in HUA mice. 469

It is worth noting that the HUA mouse model was  
470 constructed using POX and adenine. POX was used to inhibit  
471 uricase and thus increase the level of uric acid *in vivo*, whereas  
472 adenine was used to increase purine intake and simulate HUA  
473 nephropathy.<sup>11</sup> Therefore, when preparing HUA mice, it is  
474 necessary to consider the activity of the active peptide. It is  
475 possible that the sample may decrease uric acid by  
476 antagonizing POX and or enhancing uricase. In this research,  
477 the novel peptide not only inhibited XOD activity but also  
478 reduced URAT1 expression. Therefore, it could be concluded  
479 that part of the role of RDP3 in reducing uric acid comes from  
480 its influence on the production and excretion of uric acid. In  
481 addition, at present, there is no approved antihyperuricemic  
482 medicine that can both inhibit XOD activity and decrease the  
483 expression of URAT1. Even for published antihyperuricemic  
484 peptides, a similar ability to decrease uric acid through multiple  
485 targets, as found for RDP3, has not been reported.<sup>11–13,18–20</sup>  
486 Thus, these results suggest that RDP3 has great potential in the  
487 development of new drugs for the treatment of gout. 488

**RDP3 Reduced Inflammation in Kidneys of HUA  
489 Mice.** The accumulation of uric acid in the kidney can cause  
490 repeated inflammation and subsequent renal injury.<sup>33</sup> Inflam-  
491 mation plays an important role in the development of HUA  
492 nephropathy, which is a common and serious complication of  
493 gout.<sup>34</sup> In HUA, excessive accumulation of uric acid stimulates  
494 the action of the NLR family, including the pyrin domain  
495 inflammatory complex (composed of NLRP3, ASC, and  
496 procaspase-1). The assembled NLRP3 inflammasome can  
497 cause secretion of mature IL-1 $\beta$ , which is the main cause of  
498 renal injury in HUA.<sup>35–37</sup> 499

As shown in Figure 4D, the level of IL-1 $\beta$  in the model  
500 group increased significantly compared with that in the control  
501 group, indicating that HUA led to an increase in the  
502 inflammatory response of mice. Both Allo (10 mg/kg) and  
503 RDP3 treatment (100  $\mu$ g/kg, 500  $\mu$ g/kg, and 1 mg/kg)  
504 successfully reduced this inflammatory response with RDP3  
505 (500  $\mu$ g/kg and 1 mg/kg), exhibiting better anti-inflammatory  
506 ability than Allo. 507

Western blot analysis was used to detect NLRP3  
508 inflammasome expression (NLRP3, ASC, and caspase-1) in  
509 the kidneys of mice. As shown in Figure 4E–H, the NLRP3,  
510 ASC, and caspase-1 contents in the kidneys of the model group  
511 were significantly higher than those of the Allo group,  
512 suggesting that the NLRP3 inflammasome was activated. In  
513 the RDP3 groups (500  $\mu$ g/kg and 1 mg/kg), NLRP3  
514 inflammasome expression (NLRP3, ASC, and caspase-1)  
515 decreased significantly. These results show that RDP3 may  
516 reduce inflammation by inhibiting NLRP3 inflammasome  
517 expression to alleviate renal damage. 518

**RDP3 Showed Analgesic and Anti-inflammatory  
519 Activity.** Long-term HUA will increase the crystallization  
520 risk of urate in circulation, which may be deposited in joints,  
521 causing severe pain, joint deformity, and reduced quality of  
522 life.<sup>1,38</sup> Gout is a disease caused by the secretion of  
523 inflammatory cytokines, such as IL-1 $\beta$  and TNF- $\alpha$ , which is  
524 a key point in gout treatment.<sup>38</sup> In view of the excellent anti-  
525 inflammatory ability of RDP3 in HUA nephropathy, RDP3  
526 may play a therapeutic role in the acute gout attack. 527

The effect of RDP3 on inflammatory pain was detected. As  
528 seen in Figure S4, RDP3 showed significant and concentration-  
529

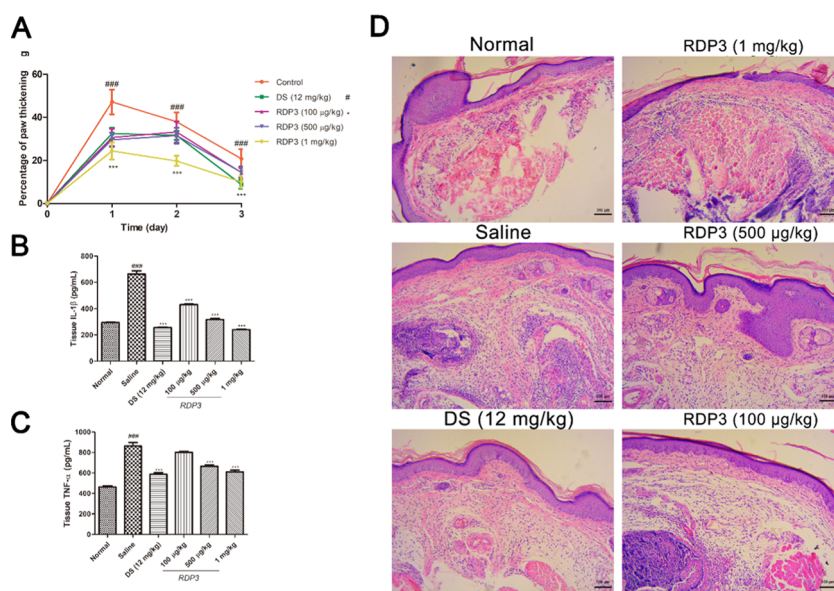


**Figure 5.** RDP3 reduced foot swelling in mice injected with MSU and decreased inflammation in mice. (A) RDP3 showed concentration-dependent reduction in paw swelling induced by MSU ( $n = 6$ ). (B) RDP3 (100  $\mu\text{g}/\text{kg}$ , 500  $\mu\text{g}/\text{kg}$ , and 1 mg/kg) induced a concentration-dependent decrease in IL-1 $\beta$  level in paw tissue of mice ( $n = 6$ ). (C) RDP3 (100 and 500  $\mu\text{g}/\text{kg}$ ) reduced the serum level of TNF- $\alpha$  in mice ( $n = 6$ ). (D) RDP3 alleviated tissue injury caused by MSU injection. ###/\*\*\* $P < 0.001$  is significantly different from the control (Student's  $t$ -tests).

530 dependent pain relief. Of note, the analgesic effect of RDP3 at  
531 1 mg/kg was stronger than that of DS at 12 mg/kg. As shown  
532 in Figure 5A, the paw swelling rate in mice peaked on the first  
533 day after injection. The swelling rates of the model and DS  
534 groups (12 mg/kg) were  $50.6 \pm 7.1$  and  $32.5 \pm 7.5\%$ ,  
535 respectively, suggesting that the DS group (12 mg/kg) showed  
536 significant alleviative effects on swelling caused by MSU ( $P <$   
537 0.001). The swelling rates of the RDP3 groups (100  $\mu\text{g}/\text{kg}$ ,  
538 500  $\mu\text{g}/\text{kg}$ , and 1 mg/kg) were  $30.6 \pm 8.1$ ,  $29.6 \pm 7.9$ , and  $24.4$   
539  $\pm 6.5\%$ , respectively. Thus, all RDP3 groups showed stronger  
540 anti-inflammatory swelling ability than that of DS at lower  
541 concentrations.

542 To verify the effect of RDP3 on inflammatory swelling  
543 induced by MSU, the levels of TNF- $\alpha$  and IL-1 $\beta$  in mouse feet  
544 were detected. As shown in Figure 5B,C, compared with the  
545 saline group, the RDP3 (500  $\mu\text{g}/\text{kg}$  and 1 mg/kg) and DS  
546 groups (12 mg/kg) significantly reduced the level of TNF- $\alpha$ ;  
547 the RDP3 (100  $\mu\text{g}/\text{kg}$ , 500  $\mu\text{g}/\text{kg}$ , and 1 mg/kg) and DS  
548 groups (12 mg/kg) also significantly reduced the level of IL-1 $\beta$   
549 ( $P < 0.001$  vs saline). It is worth noting that the anti-  
550 inflammatory activity of RDP3 at 1 mg/kg was better than that  
551 of DS at 12 mg/kg. H&E staining of feet also confirmed the  
552 positive effect of RDP3 on MSU injury recovery. As shown in  
553 Figure 5D, loose connective tissue edema in the model group  
554 was thickened and inflammatory cells were increased, which  
555 were significantly reduced in the RDP3 and DS groups. These  
556 results show that RDP3 not only had a significant anti-HUA  
557 ability but also showed excellent anti-inflammatory and  
558 analgesic capabilities.

559 A multifunctional anti-HUA peptide (RDP3) was identified  
560 in the current research, which not only inhibited XOD activity  
561 but also decreased URAT1 expression. RDP3 also reduced  
562 renal damage in HUA mice by decreasing NLRP3 inflamma-  
563 some expression and, at the same time, showed excellent anti-  
564 inflammatory and analgesic abilities. RDP3 not only provides a  
565 drug candidate for the research and development of antigout  
566 medicines but also suggests the potential that Yunnan-derived

*O. sativa* may be a healthy and nutritious food for patients with  
HUA and gout, which is expected to promote the development  
of the local planting industry.

## ASSOCIATED CONTENT

### Supporting Information

The Supporting Information is available free of charge at  
<https://pubs.acs.org/doi/10.1021/acs.jafc.0c02535>.

Purification of RDP3 from *O. sativa* collected from  
Yunnan, China (Figure S1); molecular docking of  
RDP3-XOD/URAT1 (Figure S2); XOD inhibition  
activity of RDP3 *in vitro* (Figure S3); RDP3 alleviated  
formalin-induced paw licking (Figure S4); hemolytic  
activity of RDP3 (Table S1); acinute toxicity of RDP3  
(Table S2) (PDF)

## AUTHOR INFORMATION

### Corresponding Authors

**Jun Sun** – Department of Anatomy and Histology &  
Embryology, Faculty of Basic Medical Science, Kunming Medical  
University, Kunming 650500, Yunnan, China; Phone: +86  
13888438589; Email: [sunjun6661@126.com](mailto:sunjun6661@126.com)

**Xinwang Yang** – Department of Anatomy and Histology &  
Embryology, Faculty of Basic Medical Science, Kunming Medical  
University, Kunming 650500, Yunnan, China; [orcid.org/0000-0003-3210-8908](https://orcid.org/0000-0003-3210-8908); Phone: +86 13577174345;  
Email: [yangxinwanghp@163.com](mailto:yangxinwanghp@163.com)

### Authors

**Naixin Liu** – Department of Anatomy and Histology &  
Embryology, Faculty of Basic Medical Science, Kunming Medical  
University, Kunming 650500, Yunnan, China

**Ying Wang** – Key Laboratory of Chemistry in Ethnic Medicine  
Resource, State Ethnic Affairs Commission & Ministry of  
Education, School of Ethno-Medicine and Ethno-Pharmacy,  
Yunnan Minzu University, Kunming 650504, Yunnan, China

600 **Lin Zeng** – Public Technical Service Center, Kunming Institute of  
601 Zoology, Chinese Academy of Sciences, Kunming 650223,  
602 Yunnan, China  
603 **Saige Yin** – Department of Anatomy and Histology &  
604 Embryology, Faculty of Basic Medical Science, Kunming Medical  
605 University, Kunming 650500, Yunnan, China  
606 **Yan Hu** – Department of Anatomy and Histology &  
607 Embryology, Faculty of Basic Medical Science, Kunming Medical  
608 University, Kunming 650500, Yunnan, China  
609 **Shanshan Li** – Department of Anatomy and Histology &  
610 Embryology, Faculty of Basic Medical Science, Kunming Medical  
611 University, Kunming 650500, Yunnan, China  
612 **Yang Fu** – Department of Anatomy and Histology &  
613 Embryology, Faculty of Basic Medical Science, Kunming Medical  
614 University, Kunming 650500, Yunnan, China  
615 **Xinping Zhang** – Department of Anatomy and Histology &  
616 Embryology, Faculty of Basic Medical Science, Kunming Medical  
617 University, Kunming 650500, Yunnan, China  
618 **Chun Xie** – Department of Anatomy and Histology &  
619 Embryology, Faculty of Basic Medical Science, Kunming Medical  
620 University, Kunming 650500, Yunnan, China  
621 **Longjun Shu** – Key Laboratory of Chemistry in Ethnic Medicine  
622 Resource, State Ethnic Affairs Commission & Ministry of  
623 Education, School of Ethno-Medicine and Ethno-Pharmacy,  
624 Yunnan Minzu University, Kunming 650504, Yunnan, China  
625 **Yilin Li** – Department of Anatomy and Histology & Embryology,  
626 Faculty of Basic Medical Science, Kunming Medical University,  
627 Kunming 650500, Yunnan, China  
628 **Huilong Sun** – Department of Anatomy and Histology &  
629 Embryology, Faculty of Basic Medical Science, Kunming Medical  
630 University, Kunming 650500, Yunnan, China  
631 **Meifeng Yang** – Department of Anatomy and Histology &  
632 Embryology, Faculty of Basic Medical Science, Kunming Medical  
633 University, Kunming 650500, Yunnan, China

634 Complete contact information is available at:  
635 <https://pubs.acs.org/10.1021/acs.jafc.0c02535>

### 636 Author Contributions

637 <sup>||</sup>N.L. and Y.W. contributed equally to this work

### 638 Notes

639 The authors declare no competing financial interest.

### 640 ACKNOWLEDGMENTS

641 This work was supported by grants from the Yunnan Applied  
642 Basic Research Project Foundation (2019FB128 and  
643 2017FB035), the National Natural Science Foundation of  
644 China (81760648, 31460571, and 31670776), and the Yunnan  
645 Applied Basic Research Project-Kunming Medical University  
646 Union Foundation (2018FE001(-161) and 2019FE001(-020))

### 647 REFERENCES

648 (1) Chilappa, C. S.; Aronow, W. S.; Shapiro, D.; Sperber, K.; Patel,  
649 U.; Ash, J. Y. Gout and hyperuricemia. *Compr. Ther.* **2010**, *36*, 3–13.  
650 (2) Kim, S. C.; Di Carli, M. F.; Garg, R. K.; Vanni, K.; Wang, P.;  
651 Wohlfahrt, A.; Yu, Z.; Lu, F.; Campos, A.; Bibbo, C. F.; Smith, S.;  
652 Solomon, D. H. Asymptomatic hyperuricemia and coronary flow  
653 reserve in patients with metabolic syndrome. *BMC Rheumatol.* **2018**,  
654 *2*, No. 17.  
655 (3) Kuo, D.; Crowson, C. S.; Gabriel, S. E.; Matteson, E. L.  
656 Hyperuricemia and incident cardiovascular disease and noncardiac  
657 vascular events in patients with rheumatoid arthritis. *Int. J. Rheumatol.*  
658 **2014**, *2014*, No. 523897.

(4) Burns, C. M.; Wortmann, R. L. Gout therapeutics: new drugs for 659  
an old disease. *Lancet* **2011**, *377*, 165–177. 660  
(5) Li, X.; Yan, Z.; Carlstrom, M.; Tian, J.; Zhang, X.; Zhang, W.; 661  
Wu, S.; Ye, F. Mangiferin Ameliorates Hyperuricemic Nephropathy 662  
Which Is Associated With Downregulation of AQP2 and Increased 663  
Urinary Uric Acid Excretion. *Front. Pharmacol.* **2020**, *11*, No. 49. 664  
(6) Bao, R.; Liu, M.; Wang, D.; Wen, S.; Yu, H.; Zhong, Y.; Li, Z.; 665  
Zhang, Y.; Wang, T. Effect of Eurycoma longifolia Stem Extract on 666  
Uric Acid Excretion in Hyperuricemia Mice. *Front. Pharmacol.* **2019**,  
667 *10*, No. 1464. 668  
(7) Machado-Vieira, R.; Lara, D. R.; Souza, D. O.; Kapczinski, F. 669  
Therapeutic efficacy of allopurinol in mania associated with 670  
hyperuricemia. *J. Clin. Psychopharmacol.* **2001**, *21*, 621–622. 671  
(8) Zhou, Q.; Su, J.; Zhou, T.; Tian, J.; Chen, X.; Zhu, J. A study 672  
comparing the safety and efficacy of febuxostat, allopurinol, and 673  
benzbromarone in Chinese gout patients: a retrospective cohort 674  
study. *Int. J. Clin. Pharmacol. Ther.* **2017**, *55*, 163–168. 675  
(9) Martens, K. L.; Khalighi, P. R.; Li, S.; White, A. A.; Silgard, E.; 676  
Frieze, D.; Estey, E.; Garcia, D. A.; Hingorani, S.; Li, A. Comparative 677  
effectiveness of rasburicase versus allopurinol for cancer patients with 678  
renal dysfunction and hyperuricemia. *Leuk. Res.* **2020**, *89*, 679  
No. 106298. 680  
(10) Bensman, A. Non-steroidal Anti-inflammatory Drugs 681  
(NSAIDs) Systemic Use: The Risk of Renal Failure. *Front. Pediatr.* 682  
**2019**, *7*, No. 517. 683  
(11) Liu, N.; Wang, Y.; Yang, M.; Bian, W.; Zeng, L.; Yin, S.; Xiong, 684  
Z.; Hu, Y.; Wang, S.; Meng, B.; Sun, J.; Yang, X. New Rice-Derived 685  
Short Peptide Potently Alleviated Hyperuricemia Induced by 686  
Potassium Oxonate in Rats. *J. Agric. Food Chem.* **2019**, *67*, 220–228. 687  
(12) Murota, I.; Taguchi, S.; Sato, N.; Park, E. Y.; Nakamura, Y.; 688  
Sato, K. Identification of antihyperuricemic peptides in the proteolytic 689  
digest of shark cartilage water extract using in vivo activity-guided 690  
fractionation. *J. Agric. Food Chem.* **2014**, *62*, 2392–2397. 691  
(13) Li, Q.; Kang, X.; Shi, C.; Li, Y.; Majumder, K.; Ning, Z.; Ren, J. 692  
Moderation of hyperuricemia in rats via consuming walnut protein 693  
hydrolysate diet and identification of new antihyperuricemic peptides. 694  
*Food Funct.* **2018**, *9*, 107–116. 695  
(14) Malhan, S.; Guler, S.; Yetkin, I.; Baeten, S.; Verheggen, B. Cost- 696  
Effectiveness of Exenatide Twice Daily (Bid) Added To Basal Insulin 697  
Compared To A Bolus Insulin Add-On In Turkey. *Value Health* **2014**,  
698 *17*, No. A349. 699  
(15) Higuchi, S.; Murayama, N.; Saguchi, K.; Ohi, H.; Fujita, Y.; da 700  
Silva, N. J., Jr.; de Siqueira, R. J.; Lahlou, S.; Aird, S. D. A novel 701  
peptide from the ACEI/BPP-CNP precursor in the venom of *Crotalus* 702  
*durissus collilineatus*. *Comp. Biochem. Physiol., Part C: Toxicol.* 703  
*Pharmacol.* **2006**, *144*, 107–121. 704  
(16) Wang, Y.; Li, X.; Yang, M.; Wu, C.; Zou, Z.; Tang, J.; Yang, X. 705  
Centipede venom peptide SsmTX-I with two intramolecular disulfide 706  
bonds shows analgesic activities in animal models. *J. Pept. Sci.* **2017**,  
707 *23*, 384–391. 708  
(17) Yang, X.; Lee, W. H.; Zhang, Y. Extremely abundant 709  
antimicrobial peptides existed in the skins of nine kinds of Chinese 710  
odorous frogs. *J. Proteome Res.* **2012**, *11*, 306–319. 711  
(18) Nongonierma, A. B.; Fitzgerald, R. J. Tryptophan-containing 712  
milk protein-derived dipeptides inhibit xanthine oxidase. *Peptides* 713  
**2012**, *37*, 263–272. 714  
(19) He, W.; Su, G.; Sun-Waterhouse, D.; Waterhouse, G. I. N.; 715  
Zhao, M.; Liu, Y. In vivo anti-hyperuricemic and xanthine oxidase 716  
inhibitory properties of tuna protein hydrolysates and its isolated 717  
fractions. *Food Chem.* **2019**, *272*, 453–461. 718  
(20) Li, Y.; Kang, X.; Li, Q.; Shi, C.; Lian, Y.; Yuan, E.; Zhou, M.; 719  
Ren, J. Anti-hyperuricemic peptides derived from bonito hydrolysates 720  
based on in vivo hyperuricemic model and in vitro xanthine oxidase 721  
inhibitory activity. *Peptides* **2018**, *107*, 45–53. 722  
(21) Bian, W.; Meng, B.; Li, X.; Wang, S.; Cao, X.; Liu, N.; Yang, 723  
M.; Tang, J.; Wang, Y.; Yang, X. OA-GL21, a novel bioactive peptide 724  
from *Odorana andersonii*, accelerated the healing of skin wounds. 725  
*Biosci. Rep.* **2018**, *38*, No. BSR20180215. 726

- 727 (22) Liu, N.; Li, Z.; Meng, B.; Bian, W.; Li, X.; Wang, S.; Cao, X.;  
728 Song, Y.; Yang, M.; Wang, Y.; Tang, J.; Yang, X. Accelerated Wound  
729 Healing Induced by a Novel Amphibian Peptide (OA-FF10). *Protein*  
730 *Pept. Lett.* **2019**, *26*, 261–270.
- 731 (23) Haryono, A.; Nugrahaningsih, D. A. A.; Sari, D. C. R.; Romi, M.  
732 M.; Arfian, N. Reduction of Serum Uric Acid Associated with  
733 Attenuation of Renal Injury, Inflammation and Macrophages M1/M2  
734 Ratio in Hyperuricemic Mice Model. *Kobe J. Med. Sci.* **2018**, *64*,  
735 E107–E114.
- 736 (24) Trott, O.; Olson, A. J. AutoDock Vina: improving the speed  
737 and accuracy of docking with a new scoring function, efficient  
738 optimization, and multithreading. *J. Comput. Chem.* **2010**, *31*, 455–  
739 461.
- 740 (25) Chen, Y.; Li, C.; Duan, S.; Yuan, X.; Liang, J.; Hou, S.  
741 Curcumin attenuates potassium oxonate-induced hyperuricemia and  
742 kidney inflammation in mice. *Biomed. Pharmacother.* **2019**, *118*,  
743 No. 109195.
- 744 (26) Li, C.; Chen, M.; Li, X.; Yang, M.; Wang, Y.; Yang, X.  
745 Purification and function of two analgesic and anti-inflammatory  
746 peptides from coelomic fluid of the earthworm, *Eisenia foetida*.  
747 *Peptides* **2017**, *89*, 71–81.
- 748 (27) Parashar, P.; Mazhar, I.; Kanoujia, J.; Yadav, A.; Kumar, P.;  
749 Saraf, S. A.; Saha, S. Appraisal of anti-gout potential of colchicine-  
750 loaded chitosan nanoparticle gel in uric acid-induced gout animal  
751 model. *Arch. Physiol. Biochem.* **2019**, 1–11.
- 752 (28) Han, J.; Wang, X.; Tang, S.; Lu, C.; Wan, H.; Zhou, J.; Li, Y.;  
753 Ming, T.; Wang, Z. J.; Su, X. Protective effects of tuna meat  
754 oligopeptides (TMOP) supplementation on hyperuricemia and  
755 associated renal inflammation mediated by gut microbiota. *FASEB J.*  
756 **2020**, *34*, 5061–5076.
- 757 (29) Cui, D.; Liu, S.; Tang, M.; Lu, Y.; Zhao, M.; Mao, R.; Wang, C.;  
758 Yuan, Y.; Li, L.; Chen, Y.; Cheng, J.; Lu, Y.; Liu, J. Phloretin  
759 ameliorates hyperuricemia-induced chronic renal dysfunction through  
760 inhibiting NLRP3 inflammasome and uric acid reabsorption.  
761 *Phytomedicine* **2020**, *66*, No. 153111.
- 762 (30) Yamada, Y. Hyperuricemia associated with inborn errors of  
763 purine metabolism: screening, enzymatic and genetic diagnosis. *Nihon*  
764 *Rinsho* **2003**, *61*, 278–83.
- 765 (31) Rudnicka, R.; Bojarska, E.; Kazimierczuk, Z. Benzimidazole  
766 derivatives as potent inhibitors of milk xanthine oxidase. *Acta Pol.*  
767 *Pharm.* **2004**, *61*, 37–39.
- 768 (32) Wu, X. H.; Zhang, J.; Wang, S. Q.; Yang, V. C.; Anderson, S.;  
769 Zhang, Y. W. Riparoside B and timosaponin J, two steroidal glycosides  
770 from *Smilax riparia*, resist to hyperuricemia based on URAT1 in  
771 hyperuricemic mice. *Phytomedicine* **2014**, *21*, 1196–1201.
- 772 (33) Peng, A.; Lin, L.; Zhao, M.; Sun, B. Identifying mechanisms  
773 underlying the amelioration effect of *Chrysanthemum morifolium*  
774 Ramat. 'Boju' extract on hyperuricemia using biochemical character-  
775 ization and UPLC-ESI-QTOF/MS-based metabolomics. *Food Funct.*  
776 **2019**, *10*, 8042–8055.
- 777 (34) Singh, J. A. Gout: will the "King of Diseases" be the first  
778 rheumatic disease to be cured? *BMC Med.* **2016**, *14*, No. 180.
- 779 (35) Wang, K.; Hu, L.; Chen, J.-K. RIP3-deficiency attenuates  
780 potassium oxonate-induced hyperuricemia and kidney injury. *Biomed.*  
781 *Pharmacother.* **2018**, *101*, 617–626.
- 782 (36) Tan, J.; Wan, L.; Chen, X.; Li, X.; Hao, X.; Li, X.; Li, J.; Ding,  
783 H. Conjugated Linoleic Acid Ameliorates High Fructose-Induced  
784 Hyperuricemia and Renal Inflammation in Rats via NLRP3  
785 Inflammasome and TLR4 Signaling Pathway. *Mol. Nutr. Food Res.*  
786 **2019**, *63*, No. 1801402.
- 787 (37) Chen, L.; Lan, Z. Polydatin attenuates potassium oxonate-  
788 induced hyperuricemia and kidney inflammation by inhibiting NF-  
789 kappaB/NLRP3 inflammasome activation via the AMPK/SIRT1  
790 pathway. *Food Funct.* **2017**, *8*, 1785–1792.
- 791 (38) Di Fiore, I. J.; Holloway, G.; Coulson, B. S. Innate immune  
792 responses to rotavirus infection in macrophages depend on MAVS but  
793 involve neither the NLRP3 inflammasome nor JNK and p38 signaling  
794 pathways. *Virus Res.* **2015**, *208*, 89–97.